Low-threshold calcium current and resonance in thalamic neurons: a model of frequency preference

B. Hutcheon, R. M. Miura, Y. Yarom and E. Puil

J Neurophysiol 71:583-594, 1994. ;

Journal of Neurophysiology publishes original articles on the function of the nervous system. It is published 12 times a year (monthly) by the American Physiological Society, 9650 Rockville Pike, Bethesda MD 20814-3991. ISSN: 0022-3077, ESSN: 1522-1598. Visit our website at http://www.the-aps.org/.

JOURNAL OF NEUROPHYSIOLOGY
Vol. 71, No. 2, February 1994. *Printed in U.S.A.*

Low-Threshold Calcium Current and Resonance in Thalamic Neurons: A Model of Frequency Preference

BRUCE HUTCHEON, ROBERT M. MIURA, YOSEF YAROM, AND ERNEST PUIL
Department of Pharmacology and Therapeutics, and Department of Mathematics, The University of British Columbia, Vancouver, British Columbia, V6T 1Z3, Canada; and Department of Neurobiology, Life Science Institute, Hebrew University, Jerusalem 91904, Israel

SUMMARY AND CONCLUSIONS

1. We constructed a mathematical model of the subthreshold electrical behavior of neurons in the nucleus mediodorsalis thalami (MDT) to elucidate the basis of a Ni^{2+}-sensitive low-frequency (2–4 Hz) resonance found previously in these neurons.

2. A model that included the low- and high-threshold Ca^{2+} currents (I_T and I_L), a Ca^{2+}-activated K^+ current (I_C), a rapidly inactivating K^+ current (I_A), a voltage-dependent K^+ current which we call I_{Kx}, and a voltage-independent leak current (I_l), successfully simulated the low-threshold spike observed in MDT neurons. This model (the MDT model) and a minimal version of the model containing only I_T and I_l (the minimal MDT model) were used in the analysis.

3. An impedance function was derived for a linearized version of the MDT model. This showed that the model predicts a low-frequency (2–4 Hz) resonance in the voltage response to "small" oscillatory current inputs (producing voltage changes of <10 mV) when the membrane potential is between −60 and −85 mV.

4. Further examination of the impedances for the MDT and minimal MDT models shows that I_T underlies the frequency- and voltage-dependent resonance. The slow inactivation of I_T results in an attenuation of voltage responses to low frequencies, resulting in a band-pass behavior. The fast activation of I_T amplifies the resonance and modulates the peak frequency but does not, in itself, cause resonance.

5. When voltage responses are small (<10 mV), the strength and voltage-dependence of resonance of the minimal MDT model are determined by the steady-state window conductance, g_w, due to I_T. This steady-state conductance arises where the steady-state activation, $m_\infty^2(V)$, and inactivation, $h_\infty(V)$, curves overlap. Parallel shifts in the inactivation curve can eliminate or enhance resonance with little effect on the I_T-dependent low-threshold spike evoked after hyperpolarizing current pulses. When the peak magnitude of g_w was large, the minimal MDT model showed spontaneous oscillations at 3 Hz with amplitudes >30 mV.

6. Large oscillatory current inputs evoked significantly nonlinear voltage responses in the minimal MDT model, but the 2- to 4-Hz frequency selectivity (predicted from the linearized impedance) remained.

7. We conclude that the properties of the low-threshold Ca^{2+} current, I_T, are sufficient to explain the Ni^{2+}-sensitive 2- to 4-Hz resonance seen in MDT neurons. We speculate that this frequency preference, expressed when neurons are hyperpolarized beyond −60 mV, may play a role in the organization of low-frequency activity in the thalamus during sleep.

INTRODUCTION

In the companion paper, we examined the subthreshold voltage responses of neurons in the nucleus mediodorsalis thalami (referred to here as MDT neurons) to inputs consisting of small-amplitude oscillatory currents (Puil et al. 1994). The use of small-amplitude signals allowed us to view the input-output relationship of the neurons in terms of an electrical impedance or frequency response (Puil et al. 1986). We found that many neurons showed a *frequency selectivity*, i.e., an enhanced voltage response over a restricted range of subthreshold membrane potentials and input frequencies. This appeared as a frequency- and voltage-dependent resonant hump in the neuronal frequency response that could be blocked by antagonists of the low-threshold T-type Ca^{2+} current, I_T. These observations suggest that the presence of I_T in MDT neurons confers a frequency selectivity that is unmasked only when the neurons receive inputs within the resonant frequency range.

The frequency selectivity due to resonance contrasts with the spontaneous 0.5–4 Hz oscillations in membrane voltage sometimes observed in neurons of other thalamic nuclei (Amzica et al. 1992; Curró Dossi et al. 1992; Leresche et al. 1991; Leresche 1992; Soltesz and Crunelli 1992). These oscillations are thought to arise from an interaction between I_T and the hyperpolarization-activated cation current, I_H (McCormick and Pape 1990; McCormick and Huguenard 1992; Soltesz et al. 1991), and may support the synchronized δ-wave activity (1–4 Hz) recorded during deep sleep (Curró Dossi et al. 1992; McCormick et al. 1992; Steriade et al. 1991). However, spontaneous oscillations are not seen in all thalamic neurons in vivo (Nuñez et al. 1992) or in vitro (Jahnsen and Llinás 1984; Leresche et al. 1991; Puil et al. 1994). Thus the question arises as to whether spontaneous oscillations are necessary for low-frequency thalamic activity or whether other intrinsic properties could support this behavior. Because the resonant peak in MDT neurons occurs within the frequency range of δ-wave activity, resonance also may play a role in the organization of thalamic behavior during sleep.

Previous theoretical and experimental work using the small signal impedance approach has shown that the presence of voltage-gated currents in a cell results in various types of frequency selectivity (Clapham and DeFelice 1982; Mauro et al. 1970; Puil et al. 1986–1989). In particular, a transient inward current that activates with depolarization, such as I_T, can produce a large resonance over a narrow band of frequencies and subthreshold voltages (Koch 1984; Markevich and Sel'kov 1984). Other currents that could modify the small signal responses of thalamocortical neurons at subthreshold voltages include a transient Na^+ current (I_{Na}), a persistent Na^+ current (I_{NaP}), one rapidly

inactivating and two slowly inactivating K^+ currents (I_A, I_{K2}, and I_{As}), a hyperpolarization-activated cation current (I_H), one or more Ca^{2+}-activated K^+ currents (I_C or I_{K1}), and a high-threshold Ca^{2+} current (I_L) (see review by McCormick et al. 1992; also Huguenard and Prince 1991; McCormick 1991). Also, the conductance of the voltage-independent leak current, I_l, could affect the small signal response by fixing the resting conductance.

A recently published model, by McCormick and Huguenard (1992; MH model), of the electrical behavior of ventrobasal thalamocortical neurons combined biologically realistic versions of I_T, I_L, I_A, I_{K2}, I_C, I_H, I_{Na}, I_{NaP}, and I_l to examine the genesis of spontaneous low-frequency oscillations in these neurons (see also Huguenard et al. 1991; Huguenard and McCormick 1992; Huguenard and Prince 1991, 1992). In this paper we modify the MH model to apply to MDT neurons in the subthreshold range. This new model will be called the MDT model. We also make use of a model that contains only I_T and I_l (the minimal MDT model). Our main objective is to determine if the known properties of I_T are sufficient to account for the voltage- and frequency-dependent resonance in MDT neurons. Also, we wish to identify the properties of I_T that are important in shaping the small signal responses. We employ two different techniques to achieve these aims. First, we use a linearization procedure to derive the theoretical electrical impedance of the MDT model. The linear impedance allows us to express the frequency selectivity of the model in a mathematically compact and organized form. Its disadvantage is that the interpretation of the results holds only for the nearly linear range of membrane dynamics, i.e., for current inputs that evoke "small" voltage responses. Second, we explore the nonlinear aspects of frequency selectivity through numerical simulations.

Using these techniques, we find that I_T can account for the voltage-dependent frequency selectivity observed in MDT neurons and that the linear resonance is highly sensitive to the size of the steady-state conductance due to I_T.

METHODS

Structure of the model

We modified the MH model (McCormick and Huguenard 1992) for ventrobasal thalamocortical neurons. Their description of ionic currents as macroscopic conductances multiplied by independent activation and inactivation variables and a voltage driving force is based on the theory of Hodgkin and Huxley (1952). The neuron is considered an isopotential compartment with the individual currents in parallel with the input capacitance. We determined the value of the membrane capacitance (c_m = 400 pF) for our model from the experimentally measured time courses of responses of MDT neurons to current pulses (see Puil et al. 1994).

In the MH model, changes in membrane voltage, V, are determined from

$$c_m dV/dt = -(I_l + I_T + I_L + I_{Na} + I_{NaP} + I_H + I_A + I_{K2} + I_C) \quad (1)$$

The right-hand side of *Eq. 1* contains the contributions from the various membrane ionic currents. The leak current, I_l, is the product of a constant, voltage-independent conductance and a voltage driving force

$$I_l = \bar{g}_l \cdot (V - V_l) \quad (2)$$

where $\bar{g}_l$ is the leak conductance and V_l is the reversal potential of the leak current. Other currents in the model have a similar form except that the conductance, g, may depend on voltage and the levels of activation, m^p, and inactivation, h,

$$g = \bar{g} m^p h, \quad (3)$$

where p is a positive integer. For most currents $\bar{g}$ is a constant. In the case of Ca^{2+} currents, the constant field equation is required (Hille 1992). This makes the maximal conductance a function of voltage

$$g_{Ca}(V) = 2P_{Ca}FV\xi \frac{[Ca^{2+}]_i - [Ca^{2+}]_o e^{-V\xi}}{(1 - e^{-V\xi})(V - V_{Ca})}, \quad \xi = \frac{F}{RT} \quad (4)$$

where P_{Ca} is the maximal permeability (in units of 10^{-6} cm^3/s), $[Ca^{2+}]_o$ and $[Ca^{2+}]_i$ are external and internal Ca^{2+} concentrations (in mM), V_{Ca} is the reversal potential for Ca^{2+}, and F, R, and T are thermodynamic quantities. (Mathematically, the expression for $\bar{g}_{Ca}(V)$ is undefined at $V = V_{Ca}$ and $V = 0$; however, the limiting values are finite and positive.)

The time courses of the activation and inactivation variables for the different currents in the model are given by relaxation equations. Each equation is characterized by a steady-state activation, $m_\infty(V)$, or inactivation, $h_\infty(V)$, that is approached exponentially if the voltage is held constant. Time constants, $\tau_m(V)$ and $\tau_h(V)$, determine the rate of approach to the steady-state values. The relaxation equations for the activation and inactivation associated with any given current are

$$dm/dt = (m_\infty(V) - m)/\tau_m(V), \quad (5)$$

and

$$dh/dt = (h_\infty(V) - h)/\tau_h(V). \quad (6)$$

Parameter values describing ionic currents

The functions describing the currents I_T, I_L, I_A, I_{K2}, and I_C in the MH model are given in McCormick and Huguenard (1992) and Huguenard and McCormick (1992). For the most part, these functions are derived from voltage-clamp experiments on isolated thalamic neurons (Huguenard et al. 1991, 1992). In thalamic neurons, a Ca^{2+}-activated K^+ current and a high-threshold Ca^{2+} current have been observed, but are not well characterized. Therefore, the MH model uses an I_C from the bullfrog sympathetic ganglion (Yamada et al. 1989) and an I_L from guinea pig CA3 hippocampal pyramidal neurons (Traub et al. 1991). In adapting the MH model to MDT neurons, we changed only the parameter values in the activation and inactivation equations. The changes in the parameter values needed to fit the data from MDT neurons are given in RESULTS and summarized in APPENDIX A. The values of the maximal conductance for all currents were scaled by the capacitance to keep the conductance density in our model the same as in the MH model.

Adjustments to I_T

We found that the value of P_T necessary to replicate the modeled current traces in Fig. 1 of Huguenard and McCormick (1992), or the voltage-clamp data on which the MH model is based (Huguenard and Prince 1992), was 10^{-9} times the value used in the MH model [as reported in Table 1 of McCormick and Huguenard (1992)]. Therefore, in determining the parameter values for I_T to be used in this paper, we decided to rely strictly on the empirical data reported for dissociated thalamic neurons in Huguenard and Prince (1992) and Huguenard and McCormick (1992) and apply the same compensations for temperature, charge screening effects, and cell size used in the MH model. No special changes were made in the parameters of I_T to accommo-

date MDT neurons (see APPENDIX A). In our model, as in the MH model, the maximal permeability, P_L, for the high-threshold Ca^{2+} current is set equal to twice P_T.

Effects of temperature

The calculations in this paper are for 34°C. Following Coulter et al. (1989) and McCormick and Huguenard (1992), we assume a Q_{10} of 3 for the inactivation kinetics and maximal permeability of I_T, and a Q_{10} of 5 for its activation kinetics. For all other currents we use Q_{10}s of 3 for the kinetic properties and 1.6 for the maximal conductances (McCormick and Huguenard 1992).

Calculation of the small signal response

In theory, the response of a model to small inputs at different frequencies can be determined by numerically integrating the model for each possible input. In practice, however, it is more convenient to first linearize the model and then derive an impedance relation between current inputs and voltage responses. The impedance, $Z(\omega, V)$, is the ratio of the Fourier transform of the voltage response to the Fourier transform of the current stimulus. It is a complex-valued function of frequency and voltage and contains information about the magnitudes and the relative phases of voltage responses to small periodic current inputs. In APPENDIX B, a simplified method is used to derive the complex impedance, avoiding the use of Fourier transforms. To simplify the presentation of our results we ignore the phase shift and present only the impedance magnitude, $|Z(\omega,V)|$. The impedance magnitude, expressed as a function of input frequency and holding potential, is referred to in this paper as the *frequency response* of the model. In this paper, we compare the theoretically derived frequency response to the frequency domain measurements performed on MDT neurons using small oscillatory current inputs (Puil et al. 1994).

Numerical procedures

We used the numerical integration program PHASEPLANE (Ermentrout 1990) with the Gear integration option to calculate trajectories of the solutions of mathematical models. A simulated 300-ms run takes <4 s on a 33-MHz 486 PC. We found that a tolerance of 0.01 (for the Gear integration method in PHASEPLANE) resulted in accurate computations; this agrees with the observations of Wang et al. (1991), who used the same program to integrate a less complex model involving I_T. The impedance functions were calculated with the Windows version of MathCad.

RESULTS

Estimation of model parameters

In this section we produce a model of the observed subthreshold electrical behavior of MDT neurons by modifying the empirically derived MH model (McCormick and Huguenard 1992). As detailed in the INTRODUCTION, the MH model includes I_T, I_L, I_A, I_{K2}, I_C, I_H, I_{Na}, I_{NaP}, and I_l. We can neglect the contributions of the Na^+ currents, I_{Na}, and I_{NaP}, because the data relevant to this study were collected in the presence of tetrodotoxin (TTX). Also, most MDT neurons did not show large voltage sags in response to hyperpolarizing current pulses (Puil et al. 1994), suggesting that the hyperpolarization-activated cation current, I_H, is often absent in MDT neurons. Therefore, we excluded I_H from the model but will deal with its possible role in the frequency selectivity of thalamic neurons in the DISCUSSION. Eliminating I_{Na}, I_{NaP}, and I_H results in a model

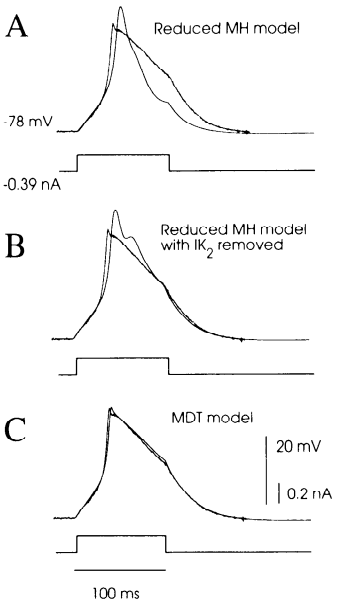

FIG. 1. Alteration of the McCormick and Huguenard (MH) model to fit data from mediodorsalis thalami (MDT) neurons. Simulated voltage transients for different versions of the MH model are compared with the low-threshold spike evoked in MDT neurons stimulated with 100-ms, 0.16-nA current pulses and treated with 0.5 μM tetrodotoxin (TTX). *A*: comparison of the low-threshold spike from an MDT neuron and the reduced version of the MH model (explained in the text). *B*: removal of I_{K2} from the reduced MH model improves the fit of the descending portion of the low-threshold spike. *C*: replacing I_{K2} with I_{Kx} leads to a good fit of the low-threshold spike. The altered model is called the MDT model in the text. Parameter values for the MDT model are given in APPENDIX A.

(the reduced MH model) that contains I_T, I_L, I_A, I_{K2}, I_C, and I_l.

Figure 1*A* compares the voltage output from the reduced MH model and the low-threshold spike evoked in MDT neurons by 100-ms current pulses. A $\bar{g}_l$ of 16 nS is used to match the initial passive phase of the response. The model produces a low-threshold spike of considerably shorter duration than seen experimentally. The rapid repolarization of the low-threshold spike is due to I_{K2}, which has much of its activation range over relatively negative potentials. We found that the reduced MH model cannot duplicate the long-lasting low-threshold spike observed in MDT neurons as long as an appreciable I_{K2} is present. Figure 1*B* shows that the complete removal of I_{K2} considerably improves the fit of the falling phase of the low-threshold spike. However, the lack of a good fit near the peak indicates that a functional equivalent of a delayed rectifier current is still required.

Therefore, we decided to change I_{K2} by making the fewest parameter changes compatible with a reasonable fit of the data. The altered current is called I_{Kx} to distinguish it from the experimentally determined I_{K2}. Replacement of I_{K2} by I_{Kx} is the only change made to the voltage-dependent properties of the reduced MH model other than the adjustments noted in METHODS. APPENDIX A gives the equations and parameter values (at 34°C) for the final model (the MDT model) containing I_T, I_L, I_A, I_{Kx}, I_C, and I_l.

The excellent agreement between the modeled and experimental low-threshold spike in Fig. 1*C* suggests that the equations and parameter values we used for I_T are accept-

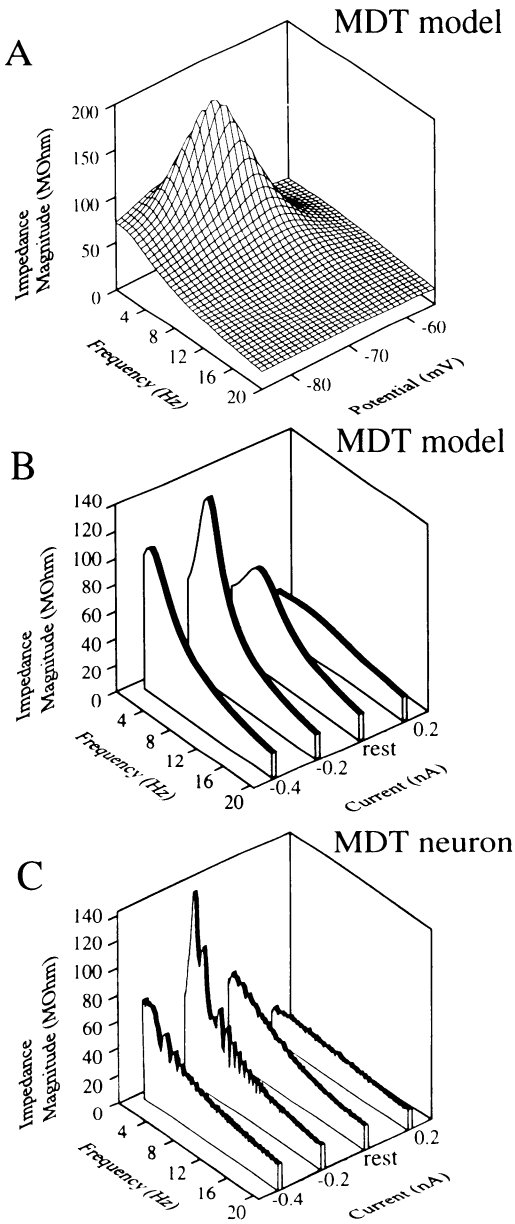

FIG. 2. Theoretical frequency response of the linearized MDT model and comparison with the measured frequency response of an MDT neuron. *A*: theoretical frequency response as a function of membrane voltage and stimulation frequency showing a large resonant hump with a peak near 4 Hz and −70 mV. *B*: frequency response of the MDT model at 4 levels of DC hyperpolarization or depolarization. *C*: observed frequency response of an MDT neuron.

able approximations for the properties of the low-threshold Ca^{2+} current in MDT neurons. Although different parameter combinations for I_T and the other ionic currents also may produce a similarly good fit, we stress that the equations and parameters that describe I_T in the MDT model are completely determined from voltage-clamp experiments in thalamic neurons (Huguenard and McCormick 1992; Huguenard and Prince 1992).

Frequency response of the MDT model

We calculated the impedance magnitude for the MDT model using *Eq.* B*24* from APPENDIX B. Figure 2*A* shows a plot of the result. A resonant hump with a peak in the 2- to 4-Hz range near −70 mV occurs in the impedance magnitude surface. Figure 2B shows the calculated frequency response at four holding currents. This can be compared with the experimentally measured frequency response of an MDT neuron at four similar holding currents shown in Fig. 2*C*. The plots show qualitative agreement between the predicted and observed responses with regard to the voltage and frequency dependence as well as the relative amplitude of the resonant hump.

Contribution of I_T to the impedance

We tested the contribution of I_T to the impedance and the resonant properties of the MDT model in two different ways: by eliminating I_T from the model (Fig. 3*A*) and, following Wang et al. (1991), by creating a minimal MDT model with only two currents, I_T and I_l (Fig. 3*B*). A comparison of Figs. 2*A* and 3*A* shows that eliminating I_T abolishes the resonant hump. We observed the same effect biologically after application of either Ni^{2+} or octanol, two

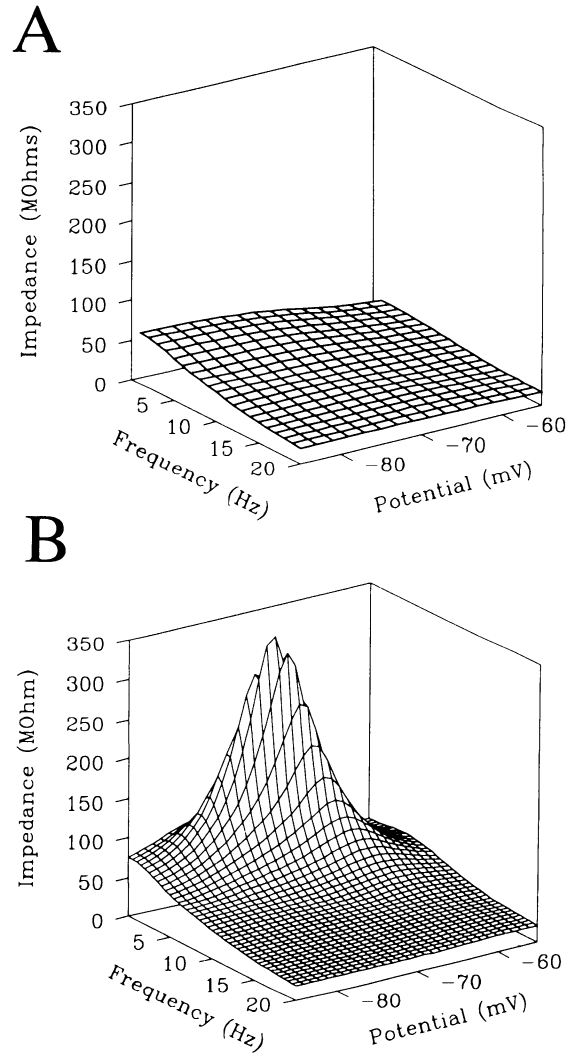

FIG. 3. I_T is sufficient to explain the resonant properties of the frequency response in the MDT model. *A*: resonance is lost when I_T is eliminated from the model. This is comparable to the block of I_T by Ni^+ or octanol. *B*: resonant frequency response of a minimal model containing only I_T and I_l.

blockers of I_T (cf. Puil et al. 1994). In contrast, the impedance surface of the minimal MDT model had a resonant hump with approximately the same voltage and frequency dependence as for the MDT model but with an even larger peak magnitude (cf. Figs. 2*A* and 3*B*).

We conclude that I_T determines the qualitative nature of the resonance that appears in the MDT model. By extension, we predict that I_T is sufficient to account for the basic properties of the low frequency resonance observed at subthreshold potentials in MDT neurons.

Mechanism of I_T resonance

Figure 4A shows how the characteristic features of I_T resonance (the drop-off in the voltage response at low frequencies and the amplification of the response near the peak frequencies) are revealed when a swept frequency current input like an impedance amplitude profile (ZAP) function (see Puil et al. 1994) is used to stimulate the minimal MDT model. The largest voltage response occurs near the same frequency (3–4 Hz) as the peak of the impedance surface in Fig. 3*B* (the resting potential in Fig. 4*A* is −71 mV with DC injection of 0.23 nA). Figure 4*A* also shows how inactivation (h) and activation (m^2) contribute to the resonance. At low frequencies the slow h variable is able to track the oscillating input and oppose large voltage changes. At higher frequencies, h cannot follow the voltage and part of its influence is lost. In contrast, m^2 is a fast variable and acts to amplify the voltage response of the model at all frequencies in Fig. 4*A*. The m^2 trace in Fig. 4*A* has a resonant shape not because it is causing the resonance directly but because it is acting as a follower and amplifier of the voltage. Thus, it is the slow inactivation of I_T that is responsible for the drop-off in response at low frequencies that characterizes resonance whereas the fast activation of I_T is responsible for the amplification near the peak frequencies.

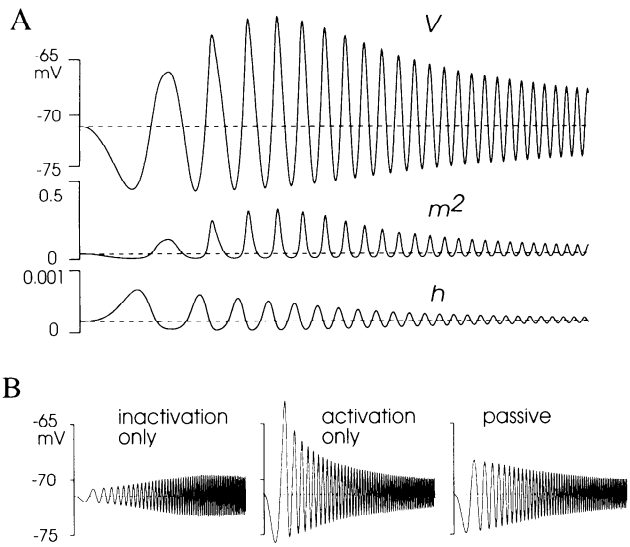

FIG. 4. Responses of the minimal MDT model to simulated impedence amplitude profile (ZAP) current inputs. *A*: voltage response (*top*) of the minimal MDT model when the frequency of the input is swept from 0 to 10 Hz over 5 s. The largest voltage response is near 4 Hz. The *middle trace* shows the time course of the activation variable, m^2, during the response. The *bottom trace* shows the time course of the inactivation variable, h. *B*: voltage responses demonstrating that I_T inactivation is responsible for resonance. Peak-to-peak magnitude of 0–15 Hz, 7.5 s, ZAP input is 0.05 nA. When only I_T inactivation is operational (*left*, activation held constant at $m^2 = 1$) the response is resonant with a peak near 10 Hz. An I_T with only activation (*middle*, inactivation held constant at $h = 1$) does not produce resonance, but there is an overall amplification of the response compared with the passive case with no I_T (*right*). The maximal permeabilities have been adjusted to produce similar responses at 15 Hz (*left*, $P_T = 0.005 \times 10^{-6}$ cm^3/s; *middle*, $P_T = 0.0003 \times 10^{-6}$ cm^3/s; *right*, $P_T = 0 \times 10^{-6}$ cm^3/s).

To clarify these points further, we have separated out the effects of I_T activation and inactivation in Fig. 4*B*. The *left trace* shows that when I_T activation is held constant at $m^2 = 1$, i.e., the voltage dependence of activation is eliminated, a frequency selectivity and low-frequency drop-off of the response is still present due to inactivation. Conversely, when inactivation is held constant at $h = 1$ (Fig. 4*B*, *middle trace*) there is no resonance. A comparison with the passive case, however, shows that there is an overall enhancement of the voltage response (*rightmost trace* in Fig. 4*B*). The combination of the amplifying effect of I_T activation and the frequency selectivity due to inactivation results in the resonant behavior of the MDT model.

Significance of the steady-state window conductance, g_w

The expression for the impedance of the MDT model given by *Eq.* B*24* suggests that the resonance associated with I_T should be particularly sensitive to certain parameter combinations corresponding to fundamental properties of the T conductance. This can be demonstrated by considering *Eq.* B*18* for the impedance of the minimal MDT model, which can be written in simplified form as

$$Z(\omega, V) = \frac{1}{\bar{g}_l + i\omega c_m + g_w(V)(\text{frequency-dependent terms due to } I_T)} \quad (7)$$

where the frequency (in Hz) is $\omega/2\pi$. The "window" conductance, g_w, arises when the steady-state activation and inactivation curves for I_T overlap and is given by

$$g_w(V) = \bar{g}_T(V) m_\infty^2(V) h_\infty(V) \quad (8)$$

Figure 5 shows graphically how the voltage dependence of the window conductance (and window current) depends on the overlap between the tails of the m_∞^2 and h_∞ curves of the low-threshold calcium conductance in the MDT model.

The importance of the window conductance is seen in *Eq. 7* where all of the contributions from I_T to the impedance are multiplied by g_w. This means that the effects of I_T will be small where g_w is close to zero. Therefore, the resonant response of the model to small oscillatory current inputs depends critically on the steady-state components of I_T. This result holds for situations where the voltage outputs are small enough that the behavior of the membrane is close to linear (<10 mV peak-to-peak in the MDT model).

Because linear resonance depends on g_w, the resonant properties of the MDT model are highly sensitive to small changes in the voltage dependence of I_T inactivation. Altering the overlap between the steady-state activation and inactivation curves for I_T changes g_w. Figure 6 shows that the

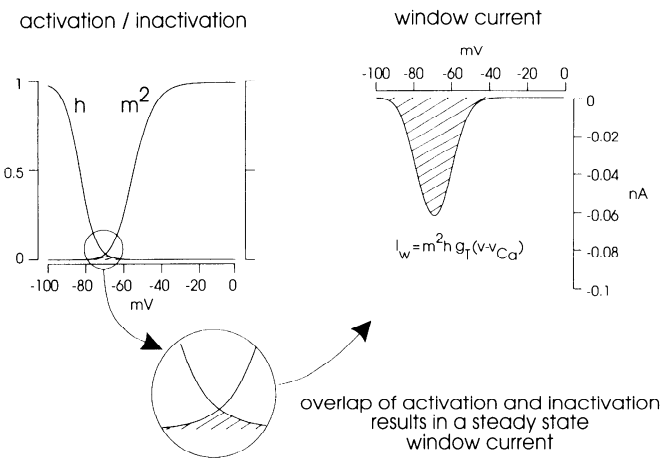

FIG. 5. Graphical explanation of the steady-state window current (I_w) corresponding to the steady-state window conductance, g_w. The window conductance arises where the steady-state activation and inactivation curves for I_T overlap.

effect of shifting the steady-state half-inactivation, $V_{h/2}$, in the MDT model from −84 mV (Fig. 6*A*) to −87 mV (Fig. 6*B*) is to reduce the peak amplitude of g_w (panels on the right in Fig. 6, *A* and *B*) and almost eliminate the resonant hump in the frequency response (panels on the left in Fig. 6, *A* and *B*). Thus a change in g_w effectively transforms the linear frequency response of the model neuron from a band-pass to a low-pass filter.

Dissociation of resonance and the low-threshold spike

Although a −3-mV shift in $V_{h/2}$ essentially abolishes the resonant properties of the MDT model, it has relatively minor effects on the rebound low-threshold spike after a hyperpolarization. Figure 7*A* shows the linear frequency response of the resonant and nonresonant versions of the MDT model (corresponding to Fig. 6, *A* and *B*, respectively) at −73 mV. The response of the nonresonant MDT model is almost the same as the passive response (· · · · ·, Fig. 7*A*). In contrast, the rebound low-threshold spike produced by a hyperpolarizing pulse is only slightly attenuated and delayed. Thus, a prediction of the model is that linear resonance and the rebound low-threshold spike can be dissociated even though they both depend on I_T.

Spontaneous oscillations in the MDT model

Large (30 mV), spontaneous, 2- to 3-Hz oscillations develop for the MDT model when the resting potential is set to −75 mV and the overlap between the activation and inactivation curves is increased by making $V_{h/2}$ more positive than −79 mV. These oscillations do not develop if the resting potential is set to −60 mV. A similar phenomenon has been described previously for a minimal model of I_T in a thalamic neuron (Wang et al. 1991). The similarity between the frequency of the spontaneous oscillations and the frequency of the resonant peak in the MDT model suggests that thalamic neurons may have multiple operating modes

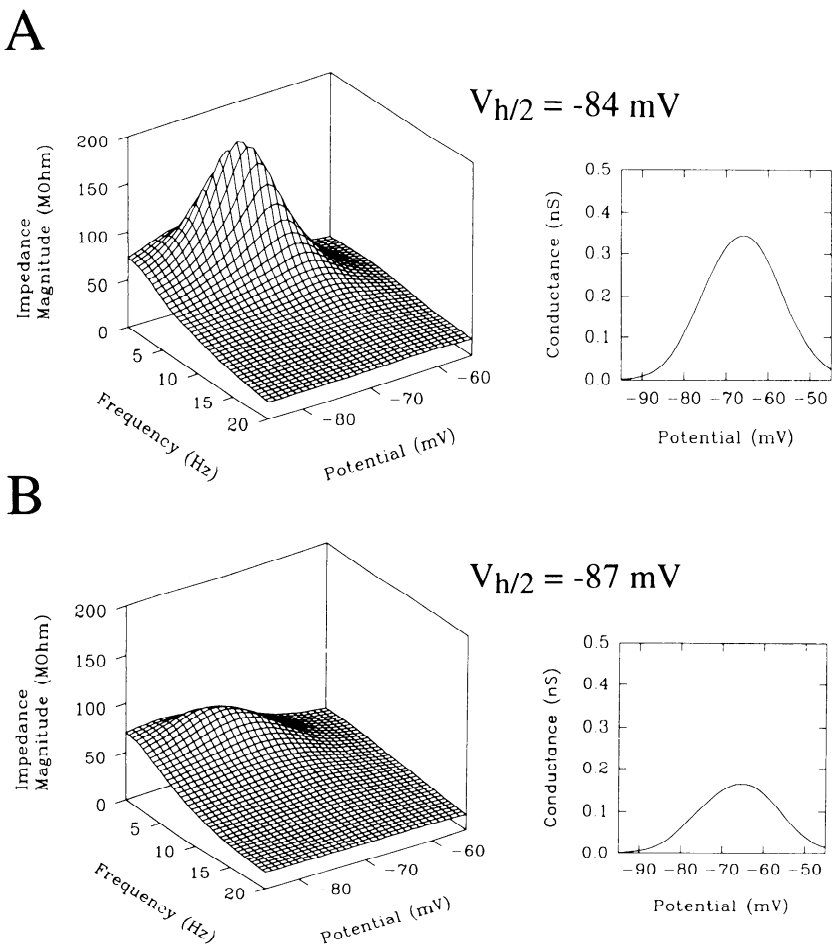

FIG. 6. The resonant hump in the frequency response surface of the MDT model is extremely sensitive to changes in the overlap of the steady-state activation and inactivation curves. *A*: frequency response of the resonant MDT model (*left*) with $V_{h/2}$ = −84 mV, and the window conductance, g_w (*right*). *B*: shifting $V_{h/2}$ by −3 mV results in a smaller g_w and almost eliminates the resonance.

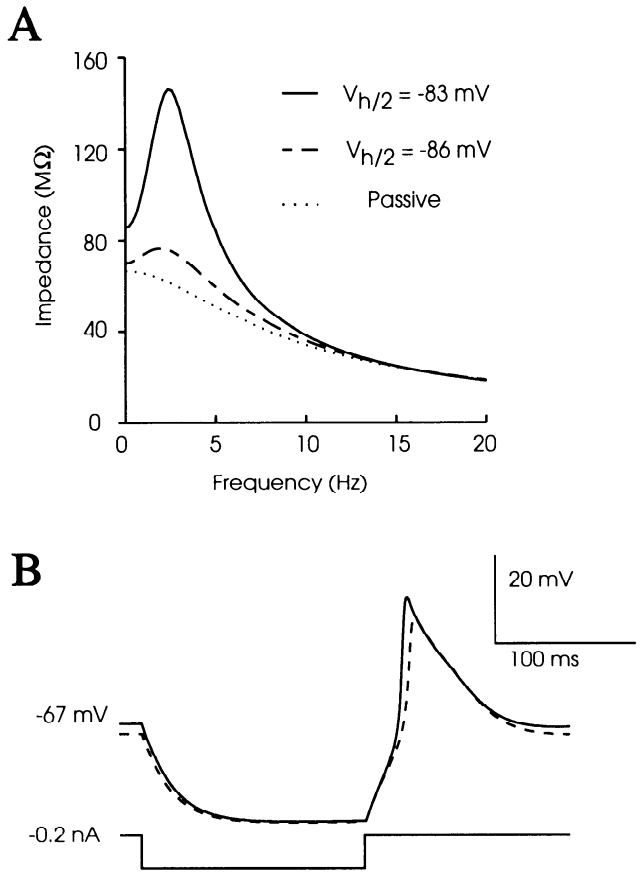

FIG. 7. Changing $V_{h/2}$ has a large effect on the resonant hump in the frequency response, but a much smaller effect on the rebound low-threshold spike after a hyperpolarization. *A*: frequency response of the MDT model at −73 mV. Shifting $V_{h/2}$ from −84 mV (——) to −87 mV (- - -) decreases the size of the resonant hump. For comparison, the frequency response of the model when I_T is eliminated entirely is also shown (· · · · ·). *B*: the rebound low-threshold spike is practically unaffected by the shift in $V_{h/2}$.

controlled by small changes in the voltage-sensitive properties of I_T.

Frequency response of the nonlinear model

Our results show that I_T is sufficient to explain the frequency preference of MDT neurons when stimulated with small periodic currents. The question arises, however, whether large oscillatory inputs that strongly engage the nonlinear properties of neurons can produce a frequency selectivity. We investigated this by stimulating the minimal MDT model with ZAP current inputs of different amplitudes (Fig. 8). The voltage responses in Fig. 8 extend from small nearly linear responses (Fig. 8, *A* and *B*; *bottom panels*) to responses that contain large nonlinear components (Fig. 8*A*; *top panel*). Figure 8*A* shows that in the resonant minimal MDT model with $V_{h/2}$ = −84 mV, and hence a large g_w, the frequency selectivity of the neuron is accentuated when a ZAP current input just large enough to evoke nonlinear Ca^{2+} spikes is used (*middle panel*). When an even larger input is used, the low-frequency components of the input also are able to evoke Ca^{2+} spikes. Figure 8*B* shows that the accentuation of the frequency preference is also present in the nonresonant minimal MDT model with $V_{h/2}$ = −87 mV (and hence a small g_w). A large enough input to this nonresonant model will produce Ca^{2+} spikes (not shown) as in the *top panel* of Fig. 8*A*. We conclude that there is a region of nonlinear enhancement of the frequency selectivity due to I_T. However, this effect is diminished for inputs that are large enough to allow the full expression of the Ca^{2+} spiking mechanism at low frequencies. Thus, both the input current amplitude and g_w can control the appearance of frequency selectivity in neurons containing I_T.

DISCUSSION

I_T underlies low-frequency resonance in MDT neurons

We have shown that the properties of the low-threshold Ca^{2+} current, I_T, can account for the experimentally observed frequency- and voltage-dependent resonance of MDT neurons. Different properties of I_T control different aspects of the resonance. The steady-state window conductance, g_w, associated with I_T, controls the voltage dependence and overall magnitude of the small signal resonance. The combination of the passive membrane properties of the neuron and the voltage dependence and kinetics of I_T inactivation determines the characteristic frequency selectivity of resonance. The fast voltage-dependent activation of I_T amplifies voltage responses throughout the resonant frequency range and modulates the location of the peak frequency but does not, in itself, cause resonance.

We found that the frequency selectivity associated with I_T resonance is retained in the minimal MDT model when current inputs large enough to evoke nonlinear low-thresh-

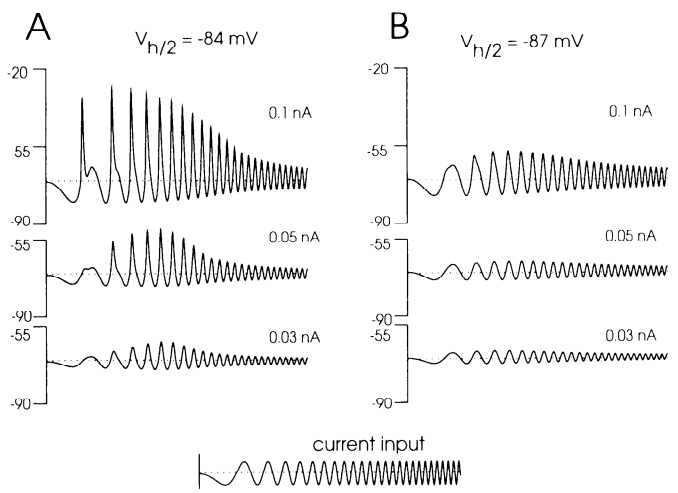

FIG. 8. Frequency selectivity is present when large current inputs are used to evoke significantly nonlinear voltage responses in the minimal MDT model. The frequency of the ZAP current input (*bottom*) is swept from 0 to 10 Hz in all cases. The peak-to-peak amplitude of the input is given above the individual voltage traces. *A*: resonant version of the minimal MDT model ($V_{h/2}$ = −84 mV). As the amplitude of the input current is increased, the frequency selectivity due to I_T resonance (almost-linear response, *bottom trace*) is first enhanced (*middle trace*) then reduced (*top trace*) as large Ca^{2+} spikes are elicited. *B*: the nonresonant minimal MDT model with $V_{h/2}$ = −87 mV and small g_w. This model is less sensitive than the resonant model to the oscillatory inputs; however, the 0.1-nA input evokes an enhanced frequency selectivity. A 0.25-nA input (not shown) produces all-or-none Ca^{2+} spikes similar to the response to the 0.1-nA input in *A*.

old Ca^{2+} spikes were used. Wang et al. (1991) also have employed a minimal model to explore the frequency dependence of low-threshold Ca^{2+} spikes in thalamic neurons. Their model uses a more complex inactivation scheme for I_T than the minimal MDT model. Our results are similar to theirs inasmuch as we also found that a slow time constant associated with I_T inactivation restricts the maximal frequency for repetitive activation of low-threshold Ca^{2+} spikes to less than $\approx$10 Hz for large current inputs (cf. *top panel* in Fig. 8*A* of this paper and Fig. 8*B* of Wang et al. with $p/P_0 = 0.5$). However our results also show that, for slightly smaller current inputs, low-threshold Ca^{2+} spikes are attenuated at low frequencies (<3 Hz; see *middle panel* of Fig. 8*A*).

The frequency preference characteristic of I_T resonance also may appear as spontaneous oscillations similar to those described in thalamic neurons in vivo (Curró Dossi et al. 1992; Nunez et al. 1992) and in vitro (Leresche et al. 1991; McCormick and Pape, 1990). In the MDT model, spontaneous oscillations occur near the resonant frequency when g_w is large. This suggests that low-frequency resonance in thalamic neurons is one aspect of a wide range of I_T-dependent properties including low-pass filter behavior and spontaneous oscillations.

Dissociation of resonance and the low-threshold spike

The MDT model shows that linear resonance depends critically on the size of g_w, whereas the low-threshold spike is less sensitive. When large oscillatory inputs that evoke nonlinear voltage responses are used, the frequency selectivity does not depend as much on the size of g_w. Pharmacological agents that selectively alter g_w, possibly by shifting the steady-state activation and inactivation curves of I_T, should change the linear resonant properties of MDT neurons but not their ability to generate a rebound low-threshold spike. Some antagonists of I_T in nonthalamic cells shift $V_{h/2}$ in the hyperpolarizing direction as well as reducing g_T (Chen et al. 1990; Miyake et al. 1992; Takahashi and Akaike 1991). In guinea pig inferior olivary neurons, harmaline shifts the I_T inactivation curve to the right without reducing g_T (Llinás and Yarom 1986). Also, investigations on a low-threshold Ca^{2+} channel α_1 subunit cloned from rat hippocampal cells and expressed in *Xenopus* oocytes, show that $V_{h/2}$ and $V_{m/2}$ can be altered by addition of rat brain Ca^{2+} channel β_1 subunits (Soong et al. 1993), independent of whole-cell peak current. This raises the possibility that pharmacological agents or endogenous substances may have differing effects on thalamic function depending on the degree to which they alter resonance or the rebound low-threshold spike.

Causes of resonance

We have shown that it is the voltage-dependent inactivation of I_T that establishes the basic frequency selectivity associated with subthreshold resonance in MDT neurons (in the presence of TTX) and that I_T activation magnifies and modulates the basic resonant pattern. We note that there are other voltage-dependent currents (such as I_{Na}), with both activation and inactivation, that should produce resonance under the proper conditions. But, we also note that the processes producing frequency selectivity and amplification need not always appear together as in the case of I_T. For instance, the slow voltage-dependent activation of the hyperpolarization-activated cation current, I_H, is mathematically similar to I_T inactivation. Therefore, I_H should be expected to produce a low-frequency resonance. This has been observed empirically in rat neocortical neurons (Hutcheon and Puil 1992) and neurons of nucleus ovoidalis in chick (B. Ströhmann, D. W. F. Schwarz, and E. Puil, personal communication).

Significance

In this paper and in the companion paper (Puil et al. 1994), we have shown that, in the absence of spontaneous oscillations, MDT neurons possess a frequency selectivity that depends on I_T and is expressed as a membrane resonance. This resonance is an intrinsic, voltage-dependent property of individual neurons that is expressed under specific conditions, i.e., in the presence of inputs with appropriate frequency components and at relatively negative membrane potentials. These same conditions prevail in the thalamus during deep sleep (Steriade et al. 1990). Therefore, we speculate that resonance can promote the development of low-frequency activity in the thalamus by acting as a band-pass amplifier to selectively enhance the voltage responses of cells to low-frequency synaptic inputs when the neurons have been hyperpolarized, as during sleep. Thus, for a neuron with resonance, even weak inputs that arrive within the resonant band of frequencies produce low-threshold Ca^{2+} spikes as shown in Fig. 8. In the n. mediodorsalis thalami, the effect of resonance would be to tune the nucleus to detect the arrival of 2- to 4-Hz activity from other structures and to respond with bursts of activity in the same frequency range. In neurons with little or no resonance, the voltage- and frequency-dependent amplification of signals is small or absent. Therefore, the connection between low-frequency inputs and bursts of spikes due to low-threshold Ca^{2+} spikes is weaker even though a large stimulus can still evoke a rebound low-threshold spike (Figs. 7*B* and 8*B*). Under these conditions the bursting responses of neurons would not show the sensitive dependence on membrane voltage and input frequency associated with resonance.

Taken together these properties imply that I_T resonance enhances the relationship between inputs to thalamocortical neurons and the outputs characteristic of these neurons during deep sleep. Finally, our finding that resonance is highly sensitive to the overlap of the I_T activation and inactivation curves raises the possibility that the control of 2- to 4-Hz activity in the thalamus depends on the steady-state I_T window conductance in individual thalamocortical neurons.

APPENDIX A

The MDT model uses the voltage-dependent currents I_T, I_L, I_A, I_{Kx}, I_C, and a voltage-independent leak current I_l. This appendix gives the expressions and parameter values for the currents and for

their steady-state activation (m_∞) and inactivation (h_∞) functions and the corresponding time constants (τ_m and τ_h) at 34°C. The total membrane capacitance is 400 pF, corresponding to a membrane area of 40,000 μm^2 if a specific capacitance of 1 $\mu F/cm^2$ is assumed. The maximal permeabilities and conductances are given below along with their corresponding specific values in parentheses. With the exceptions noted at the end of this appendix, the parameter values used in the MDT model are the same as those used in the MH model after appropriate scalings for temperature and membrane area (McCormick and Huguenard 1992).

I_T

$$I_T = \bar{g}_T(V) m_T^2 h_T \cdot (V - V_{Ca}) \quad (A1)$$

where $\bar{g}_T(V)$ is given by *Eq. 4* with $P_T = 0.05 \times 10^{-6}$ cm^3/s (for a specific permeability of 0.000125 cm/s, which is equivalent to 0.65 mS/cm^2 at −65 mV), $[Ca^{2+}]_0 = 2 \times 10^{-3}$ M, $\xi = 1/13$ mV^{-1}, and $F = 9.65 \times 10^4$ C/mol. $[Ca^{2+}]_i$ is a variable described below and V_{Ca} is given by the Nernst relation $V_{Ca} = 1/\xi \ln([Ca^{2+}]_0/[Ca^{2+}]_i)$.

$$m_{\infty_T}(V) = (1 + \exp((V - V_{m_{T/2}})/k_{m_T}))^{-1} \quad (A2)$$

$$h_{\infty_T}(V) = (1 + \exp((V - V_{h_{T/2}})/k_{h_T}))^{-1} \quad (A3)$$

with $V_{m_{T/2}} = -62$ mV, $V_{h_{T/2}} = -84$ mV, $k_{m_T} = -6.2$ mV^{-1}, and $k_{h_T} = 4$ mV^{-1}

$$\tau_{m_T}(V) = 0.2\{(\exp((V + 132)/-16.7) + \exp((V + 16.8)/18.2))^{-1} + 0.612\} \quad (A4)$$

$$\tau_{h_T}(V) = \begin{cases} 0.33 \exp((V + 467)/66.6) & \text{for } V < -80 \text{ mV} \\ 0.33(\exp((V + 22)/-10.5) + 28) & \text{for } V \geq -80 \text{ mV} \end{cases} \quad (A5)$$

I_L

$$I_L = \bar{g}_L(V) m_L^2 \cdot (V - V_L) \quad (A6)$$

where $\bar{g}_L(V)$ is given by *Eq. 4* with the same parameters as for I_T except that

$P_L = 2P_T = 0.1 \times 10^{-6}$ cm^3/s (0.00025 cm/s or 1.3 mS/cm^2 at −65 mV).

$$m_{\infty_L}(V) = \alpha_L(V)/(\alpha_L(V) + \beta_L(V)) \quad (A7)$$

$$\tau_{\infty_L}(V) = 0.33/(\alpha_L(V) + \beta_L(V)) \quad (A8)$$

with

$$\alpha_L(V) = 1.6/(1 + \exp(-0.072(V - 5))), \quad (A9)$$

$$\beta_L(V) = 0.02(V - 1.31)/(\exp((V - 1.3)/5.36) - 1) \quad (A10)$$

I_A

$$I_A = \bar{g}_A(0.6 m_{A_1}^4 h_{A_1} + 0.4 m_{A_2}^4 h_{A_2}) \cdot (V - V_K) \quad (A11)$$

with $\bar{g}_A = 1.33$ μS (3.3 mS/cm^2) and $V_K = -105$ mV.

$$m_{\infty_{A_i}}(V) = (1 + \exp(V - V_{m_{A_i/2}})/k_{m_{A_i}}))^{-1}, \quad i = 1, 2 \quad (A12)$$

where $V_{m_{A_1}/2} = -60$ mV, $V_{m_{A_2}/2} = -36$ mV, $k_{m_{A_1}} = -8.5$ mV, and $k_{m_{A_2}} = -20$ mV.

$$h_{\infty_{A_i}}(V) = (1 + \exp((V - V_{h_{A_i/2}})/k_{h_{A_i}}))^{-1}, \quad i = 1, 2 \quad (A13)$$

with $V_{h_{A_i}/2} = -78$ mV and $k_{h_{A_i}} = 6$ mV^{-1}.

$$\tau_{m_A}(V) = 0.33(\exp((V - 35.8)/19.7) + \exp((V - 79.7)/-12.7))^{-1} + 0.37 \quad (A14)$$

$$\tau_{h_{A_1}}(V) = 0.33\{\exp((V + 46)/5) + \exp((V + 238)/-37.5)\}^{-1}$$ for $V < -63$ mV, otherwise $\tau_{h_{A_1}} = 19$ ms (A15)

$$\tau_{h_{A_2}}(V) = 0.33\{\exp((V + 46)/5) + \exp((V + 238)/-37.5)\}^{-1}$$ for $V < -73$ mV, otherwise $\tau_{h_{A_2}} = 60$ ms (A16)

I_{K_x}

$$I_{Kx} = \bar{g}_{Kx} m_{Kx}(0.4 h_{Kx1} + 0.6 h_{Kx2}) \cdot (V - V_K) \quad (A17)$$

with $\bar{g}_{Kx} = 1.3$ μS (3.3 mS/cm^2).

$$m_{\infty_{Kx}}(V) = (1 + \exp((V - V_{m_{Kx/2}})/k_{m_{Kx}}))^{-4} \quad (A18)$$

where $V_{m_{Kx}/2} = -52$ mV and $k_{m_{Kx}} = -8$ mV.

$$h_{\infty_{K_{x_i}}}(V) = (1 + \exp((V - V_{h_{K_{x_i}/2}})/k_{h_{K_{x_i}}}))^{-1}, \quad i = 1, 2 \quad (A19)$$

where $V_{h_{K_{x_i}}/2} = -58$ mV and $k_{h_{K_{x_i}}} = 10.6$ mV.

$$\tau_{m_{Kx}}(V) = 0.033\{(\exp((V - 81)/25.6) + \exp((V + 132)/-18))^{-1} + 9.9\} \quad (A20)$$

$$\tau_{h_{K_{x_1}}}(V) = 0.33\{(\exp(V - 1329)/200) + \exp((V + 130/-7.1))^{-1} + 120\} \quad (A21)$$

The second time constant, $\tau_{h_{K_{x_2}}}$, is the same as $\tau_{h_{K_{x_1}}}$ for $V < -70$ mV, and $\tau_{h_{K_{x_2}}} = 8.9$ s for $V \geq -70$ mV.

I_C

$$I_C = \bar{g}_C m_C \cdot (V - V_K) \quad (A22)$$

where $\bar{g}_C = 1.3$ μS (3.3 mS/cm^2).

$$m_{\infty_C}(V) = \alpha_C(V)/(\alpha_C(V) + \beta_C(V)) \quad (A23)$$

$$\tau_{\infty_C}(V) = 0.33/(\alpha_C(V) + \beta_C(V)) \quad (A24)$$

with

$$\alpha_C(V) = 2.5 \times 10^5 [Ca^{2+}]_i e^{V/24} \quad (A25)$$

$$\beta_C(V) = 0.1 e^{-V/24} \quad (A26)$$

$[Ca^{2+}]_i$ *buffering*

$$d[Ca^{2+}]_i/dt = -([Ca^{2+}]_i - \phi)/\tau_{Ca} + \zeta I_L \quad (A27)$$

where $\tau_{Ca} = 1$ ms is the Ca^{2+} buffering time constant, $\phi = 5 \times 10^{-8}$ M is the minimal $[Ca^{2+}]_i$ value, and $\zeta = -1.29 \times 10^{-6}$ converts Ca^{2+} currents into changes in $[Ca^{2+}]_i$ in a shell 100 nm below a membrane of surface area 40,000 μm^2. I_T is assumed not to contribute to $[Ca^{2+}]_i$.

I_l

The MH model uses separate Na^+- and K^+-dependent leak conductances, g_{Naleak} and g_{Kleak}, respectively. The MDT model lumps these voltage-independent conductances into a single current

$$I_l = \bar{g}_l \cdot (V - V_l) \quad (A28)$$

with $\bar{g}_l = 0.016$ μS (0.04 mS/cm^2) and $V_l = -63$ mV.

Differences between the MDT model and the reduced MH model

The differences between the MDT model and the reduced MH model lie in the parameters for I_{Kx} activation (corresponding to

I_{K2} in the reduced MH model), the maximal permeability for I_T, and the maximal conductance for the voltage-independent leak current, $\bar{g}_l$ (corresponds to $g_{Naleak} + g_{Kleak}$ in the reduced MH model).

We altered the activation properties of I_{K2} to produce I_{Kx} by decreasing its time constant by a factor of 10, shifting the steady-state activation curve by −9 mV, and changing the slope factor, k_m, from −17 to −8 mV.

The P_T for the MDT model is 10^{-9} of the P_T for the MH model (see METHODS).

The summed maximal conductance of voltage-independent currents in the MH model is 0.028 μS (calculated for 34°C and an input capacitance of 400 pF). The corresponding leak conductance, g_l, for the MDT model is 0.016 μS.

APPENDIX B

In this appendix we derive an expression for the impedance of an isopotential neuron having voltage-dependent and -independent currents. We begin with the simple case of one voltage-dependent current and a leak current.

Derivation of the impedance of a neuron with a single voltage-dependent current

Assume that the electrical behavior of the neuron is described by

$$c_m dV/dt = -\bar{g}_l \cdot (V - V_l) - \bar{g}(V) m^p h^q \cdot (V - V_{rev}) + i^0_{ext} \quad (B1)$$

$$dm/dt = (m_\infty(V) - m)/\tau_m(V) \quad (B2)$$

$$dh/dt = (h_\infty(V) - h)/\tau_h(V) \quad (B3)$$

where the variables and parameters have the same meanings as in METHODS except that the identity of the voltage-gated current is unspecified so as to stress the generality of the equations. The term i^0_{ext} is a constant external current that is under the control of the investigator and used to change the resting voltage of the system.

For each value of i^0_{ext}, the system has a steady state (V_0, m_0, h_0) found by setting the time derivatives equal to zero, i.e.,

$$0 = -\bar{g}_l \cdot (V_0 - V_l) - \bar{g}(V_0) m_0^p h_0^q \cdot (V_0 - V_{rev}) + i^0_{ext} \quad (B4)$$

$$0 = (m_\infty(V_0) - m_0)/\tau_m(V_0) \quad (B5)$$

$$0 = (h_\infty(V_0) - h_0)/\tau_h(V_0) \quad (B6)$$

Many systems of the form B*1*–B*3* possess multiple equilibria with different types of stability. Here we consider only the equilibrium state with the most hyperpolarized membrane potential and assume that it is stable. Note that *Eqs.* B*5* and B*6* yield

$$m_0 = m_\infty(V_0) \quad \text{and} \quad h_0 = h_\infty(V_0) \quad (B7)$$

To proceed further, we assume that i^0_{ext} is replaced by

$$i_{ext}(t) = i^0_{ext} + \delta I(t) \quad (B8)$$

where $\delta I(t)$ is a small perturbation current. We can then linearize the equations about the point (V_0, m_0, h_0) and determine the response of the linearized system to inputs $\delta I(t)$ at different frequencies. Note that some of the nonlinear terms have linear effects that are included in the linearized system.

Introduce the perturbation variables, $v = V - V_0$, $M = m - m_0$, and $H = h - h_0$, where v, M, and H are assumed to be small. Then expand *Eqs.* B*1*–B*3* in a Taylor series in v, M, and H about (V_0, m_0, h_0) using *Eqs.* B*4*–B*7*. Neglecting the terms in the expansion that involve products of the perturbation variables yields

$$c_m dv/dt = -\bar{g}_l v - g_w(V_0)\left(p\frac{M}{m_0} + q\frac{H}{h_0} + \frac{\bar{g}'_0 v}{\bar{g}_0} + \frac{v}{(V_0 - V_{rev})}\right) \times (V_0 - V_{rev}) + \delta I(t) \quad (B9)$$

$$dM/dt = (m'_0 v - M)/\tau_{m_0} \quad (B10)$$

$$dH/dt = (h'_0 v - H)/\tau_{h_0} \quad (B11)$$

where $g_w(V_0) = \bar{g}_0 m_0^p h_0^q$ is the steady-state "window" conductance expected from voltage-operated channels at the holding potential V_0, and the subscript 0 is used to denote the value of functions at the steady state, i.e., $\bar{g}_0 = \bar{g}(V_0)$, $\tau_{m_0} = \tau_m(V_0)$, and $\tau_{h_0} = \tau_h(V_0)$. In addition we have defined $\bar{g}'_0 = (d\bar{g}/dv)(V_0)$, $m'_0 = (dm_\infty/dv)(V_0)$, and $h'_0 = (dh_\infty/dv)(V_0)$.

The linearized system approximates the behavior of *Eqs.* B*1*–B*3* when the perturbation current, $\delta I(t)$, is small. In experiments with actual neurons, the only variables that are directly measurable are $\delta I(t)$ and the perturbation output voltage $v(t)$. The relationship between these observables is described by the input impedance, defined as the Fourier transform of the voltage output divided by the Fourier transform of the current input (see Puil et al. 1994). In the case of the linear, homogeneous system *Eqs.* B*9*–B*11*, the use of Fourier transforms can be avoided by assuming that $\delta I(t)$ is a pure sinusoidal oscillation of unit amplitude at a fixed frequency, f (in Hz). For simplicity, we represent the perturbation current in complex notation, i.e., $\delta I(t) = e^{i\omega t}$, where $\omega = 2\pi f$. Because the input is at a single frequency, we look for solutions of *Eqs.* B*9*–B*11* at the same frequency in the form

$$v(t) = Ze^{i\omega t} \quad (B12)$$

$$M(t) = Ye^{i\omega t} \quad (B13)$$

$$H(t) = Xe^{i\omega t} \quad (B14)$$

Substituting these expressions into *Eqs.* B*9*–B*11* and dividing through by $\delta I(t) = e^{i\omega t}$ gives

$$i\omega c_m Z = -\bar{g}_l Z - g_w(V_0)\left(p\frac{Y}{m_0} + q\frac{X}{h_0} + \frac{\bar{g}'_0 Z}{\bar{g}_0} + \frac{Z}{(V_0 - V_{rev})}\right)(V_0 - V_{rev}) + 1 \quad (B15)$$

$$i\omega Y = (m'_0 Z - Y)/\tau_{m_0} \quad (B16)$$

$$i\omega X = (h'_0 Z - X)/\tau_{h_0} \quad (B17)$$

Finally, eliminating X and Y in *Eq.* B*15* using *Eq.* B*16* and B*17* and rearranging yields

$$Z(\omega; V_0) = \left\{\bar{g}_l + i\omega c_m + g_w(V_0)\left(p\frac{m'_0}{m_0}\cdot\frac{1}{1 + i\omega\tau_{m_0}} + q\frac{h'_0}{h_0} \times \frac{1}{1 + i\omega\tau_{h_0}} + \frac{\bar{g}'_0}{\bar{g}_0} + \frac{1}{(V_0 - V_{rev})}\right)(V_0 - V_{rev})\right\}^{-1} \quad (B18)$$

Note that the impedance coincides with Z in *Eq.* B*12* because the current input is of unit amplitude. *Equation* B*18* gives the linearized impedance of *Eqs.* B*1*–B*3* as a function of frequency for each equilibrium membrane voltage, V_0. In the remainder of this appendix and in the body of the paper, we drop the 0 subscripts for notational convenience.

Models with more than one voltage-gated current

If there are several voltage-gated currents to be considered, each can be expressed in the same form as the terms in *Eq.* B*1*, i.e.,

$$I_n = \bar{g}_n(V) m_n^{p_n} h_n^{q_n} \cdot (V - V_n), \qquad n = 1, 2, \ldots, N \quad (B19)$$

where N is the number of distinct types of voltage gated-currents, p_n and q_n are integer exponents, V_n is the reversal potential for current I_n, and each current I_n has appropriate auxiliary equations

for its activation (m_n) and inactivation (h_n) processes similar to *Eqs.* B*2* and B*3*.

Carrying out the linearization and the small signal analysis, as above, results in an expression that is similar to *Eq.* B*18* except that there is a separate term in the denominator for each different current, i.e.

$$Z(\omega, V) = \frac{1}{\bar{g}_l + i\omega c_m + \sum_{n=1}^{N} g_{n_{ss}}(V) F_n(\omega, V)} \quad \text{(B20)}$$

where $g_{n_{ss}}(V)$ is the steady-state conductance associated with each current and the form of each term, $F_n(\omega, V)$, is given by

$$F_n(\omega, V) = \left(p_n \frac{m'_n}{m_n} \cdot \frac{1}{1 + i\omega\tau_{m_n}} + q_n \frac{h'_n}{h_n} \times \frac{1}{1 + i\omega\tau_{h_n}} + \frac{\bar{g}'_n}{\bar{g}_n} + \frac{1}{(V - V_n)} \right)(V - V_n) \quad \text{(B21)}$$

Note from *Eq.* B*20* that a current does not contribute to the impedance in a region where its steady-state conductance, $g_{n_{ss}}$, is near zero. All of the quantities with a subscript n are assumed to be evaluated at the steady-state membrane potential.

When the current does not have an instantaneous rectification, such as that described by the constant field equation, the conductance is not a function of voltage and therefore $\bar{g}'_n = 0$. In this case (B*21*) simplifies slightly to

$$F_n(\omega, V) = \left(p_n \frac{m'_n}{m_n} \cdot \frac{1}{1 + i\omega\tau_{m_n}} + q_n \frac{h'_n}{h_n} \times \frac{1}{1 + i\omega\tau_{h_n}} + \frac{1}{(V - V_n)} \right)(V - V_n) \quad \text{(B22)}$$

For an interpretation of each term in *Eq.* B*22* and its contributions to the band-pass or low-pass behavior of $Z(\omega, V)$, see Koch (1984).

Models with ion-sensitive currents

The MH and MDT models both contain a Ca^{2+}-activated K^+ current, I_C. This requires an extension of the equations above because I_C acquires part of its voltage sensitivity indirectly from Ca^{2+} influx through the high-threshold voltage-gated Ca^{2+} channel, I_L. The expressions for the currents due to I_C and I_L and the equation for Ca^{2+} buffering are given in APPENDIX A.

The derivation of the impedance is similar to the analysis above except that cross terms arise between I_L and I_C. The contribution of I_L and I_C to the sum in the denominator of *Eq.* B*20* is

$$g_{L_{ss}} F_L(\omega, V) + g_{C_{ss}} F_C(\omega, V) + g_{L_{ss}} g_{C_{ss}} \tau_{Ca} \zeta \left(p_C \frac{m_C^*}{m_C} \frac{1}{1 + i\omega\tau_{Ca}} \right) F_L(\omega, V) \quad \text{(B23)}$$

where m_C^* indicates the derivative of m_C is with respect to $[Ca^{2+}]_i$ rather than voltage.

Impedance for the MDT model

Thus the impedance of the MDT model is

$$Z(\omega, V) = \left\{ \bar{g}_l + i\omega c_m + \sum_{n=1}^{N} g_{n_{ss}}(V) F_n(\omega, V) + g_{L_{ss}} g_{C_{ss}} \tau_{Ca} \zeta \left(p_C \frac{m_C^*}{m_C} \frac{1}{1 + i\omega\tau_{Ca}} \right) F_L(\omega, V) \right\}^{-1} \quad \text{(B24)}$$

where n ranges over the currents in the MDT model as given in the paper.

This work was supported by the Medical Research Council of Canada (E. Puil and R. M. Miura), the Natural Sciences and Engineering Research Council of Canada (R. M. Miura), the United States-Israel Binational Science Foundation (Y. Yarom), and an International Scientific Exchange Award from the Natural Sciences and Engineering Research Council of Canada (Y. Yarom).

Address for reprint requests: E. Puil, The University of British Columbia, Faculty of Medicine, Dept. of Pharmacology and Therapeutics, 2176 Health Sciences Mall, Vancouver, B.C. V6T 1Z3, Canada.

Received 14 July 1993; accepted in final form 20 September 1993.

REFERENCES

AMZICA, F., NUÑEZ, A., AND STERIADE, M. Delta frequency (1–4 Hz) oscillations of perigeniculate thalamic neurons and their modulation by light. *Neuroscience* 51: 285–294, 1992.

CHEN, C., ZHANG, J., VINCENT, J. D., AND ISRAEL, J. M. Two types of voltage-dependent calcium current in rat somatotrophs are reduced by somatostatin. *J. Physiol. Lond.* 425: 29–42, 1990.

CLAPHAM, D. E. AND DEFELICE, L. J. Small signal impedance of heart cell membranes. *J. Membr. Biol.* 67: 63–71, 1982.

COULTER, D. A., HUGUENARD, J. R., AND PRINCE, D. A. Calcium currents in rat thalamocortical relay neurones: kinetic properties of the transient, low-threshold current. *J. Physiol. Lond.* 414: 587–604, 1989.

CURRÓ DOSSI, R. C., NUÑEZ, A., AND STERIADE, M. Electrophysiology of a slow (0.5–4 Hz) intrinsic oscillation of cat thalamocortical neurones in vivo. *J. Physiol. Lond.* 447: 215–234, 1992.

ERMENTROUT, G. B. *PHASEPLANE: The Dynamical Systems Tool, version 3.0.* Pacific Grove, CA: Brooks/Cole, 1990.

HILLE, B. *Ionic Channels of Excitable Membranes.* 2nd ed. Sunderland, MA: Sinauer, 1992.

HODGKIN, A. L. AND HUXLEY, A. F. A quantitative description of membrane current and its application to conduction and excitation in nerve. *J. Physiol. Lond.* 117: 500–544, 1952.

HUGUENARD, J. R., COULTER, D. A., AND PRINCE, D. A. A fast transient potassium current in thalamic relay neurons: kinetics of activation and inactivation. *J. Neurophysiol.* 66: 1304–1315, 1991.

HUGUENARD, J. R. AND MCCORMICK, D. A. Simulation of the currents involved in rhythmic oscillations in thalamic relay neurons. *J. Neurophysiol.* 68: 1373–1383, 1992.

HUGUENARD, J. R. AND PRINCE, D. A. Slow inactivation of a TEA-sensitive K current in acutely isolated rat thalamic relay neurons. *J. Neurophysiol.* 66: 1316–1328, 1991.

HUGUENARD, J. R. AND PRINCE, D. A. A novel T-type current underlies prolonged Ca^{2+}-dependent burst firing in GABAergic neurons of rat thalamic reticular nucleus. *J. Neurosci.* 12: 3804–3817, 1992.

HUTCHEON, B. AND PUIL, E. A low-frequency subthreshold resonance in neocortical neurons generated mainly by IH. *Soc. Neurosci. Abstr.* 18: 1344, 1992.

JAHNSEN, H. AND LLINÁS, R. Electrophysiological properties of guinea-pig thalamic neurones: an in vitro study. *J. Physiol. Lond.* 349: 205–226, 1984.

KOCH, C. Cable theory in neurons with active, linearized dendrites. *Biol. Cybern.* 50: 15–33, 1984.

LERESCHE, N. Synaptic currents in thalamo-cortical neurons of the rat lateral geniculate nucleus. *Eur. J. Neurosci.* 4: 595–602, 1992.

LERESCHE, N., LIGHTOWLER, S., SOLTESZ, I., JASSIK-GERSCHENFELD, D., AND CRUNELLI, V. Low-frequency oscillatory activities intrinsic to rat and cat thalamocortical cells. *J. Physiol. Lond.* 441: 155–174, 1991.

LLINÁS, R. AND YAROM, Y. Oscillatory properties of guinea pig inferior olivary neurones and their pharmacological modulation: an in vitro study. *J. Physiol. Lond.* 376: 163–182, 1986.

MARKEVICH, N. I. AND SEL'KOV, E. E. Resonance phenomena in membranes containing ionic channels with inactivation. *Biophysics* 5: 891–897, 1984.

MAURO, A., CONTI, F., DODGE, F., AND SCHOR, R. Subthreshold behavior, and phenomenological impedance of the squid giant axon. *J. Gen. Physiol.* 55: 497–523, 1970.

MCCORMICK, D. A. Functional properties of a slowly inactivating potassium current in guinea pig dorsal lateral geniculate relay neurons. *J. Neurophysiol.* 66: 1176–1189, 1991.

MCCORMICK, D. A., HUGUENARD, J., AND STROWBRIDGE, B. W. Determination of state-dependent processing in thalamus by single neuron properties and neuromodulators. In: *Single Neuron Computation,* edited by T. McKenna, J. Davis, and S. F. Zornetzer. Academic Press, 1992, p. 259–290.

McCORMICK, D. A. AND HUGUENARD, J. R. A model of the electrophysiological properties of thalamocortical relay neurons. *J. Neurophysiol.* 68: 1384–1400, 1992.

McCORMICK, D. A. AND PAPE, H. C. Properties of a hyperpolarization-activated cation current and its role in rhythmic oscillation in thalamic relay neurones. *J. Physiol. Lond.* 431: 291–318, 1990.

MIYAKE, N., WAKAMORI, M., AND AKAIKE, N. A new type of Ca^{2+} channel blocker, NC-1100, inhibits the low- and high-threshold Ca^{2+} currents in the rat CNS neurons. *Brain Res.* 598: 215–220, 1992.

NUÑEZ, A., AMZICA, F., AND STERIADE, M. Intrinsic and synaptically generated delta (1–4 Hz) rhythms in dorsal lateral geniculate neurons and their modulation by light-induced fast (30–70 Hz) events. *Neuroscience* 51: 269–284, 1992.

PUIL, E. AND GIMBARZEVSKY, B. Modifications in membrane properties of trigeminal sensory neurons during general anesthesia. *J. Neurophysiol.* 58: 87–104, 1987.

PUIL, E., GIMBARZEVSKY, B., AND MIURA, R. M. Quantification of membrane properties of trigeminal root ganglion neurons in guinea pigs. *J. Neurophysiol.* 55: 995–1016, 1986.

PUIL, E., GIMBARZEVSKY, B., AND MIURA, R. M. Voltage dependence of membrane properties of trigeminal root ganglion neurons. *J. Neurophysiol.* 58: 66–86, 1987.

PUIL, E., GIMBARZEVSKY, B., AND SPIGELMAN, I. Primary involvement of K^+ conductances in membrane resonance of trigeminal root ganglion neurons. *J. Neurophysiol.* 59: 77–89, 1988.

PUIL, E., MEIRI, H., AND YAROM, Y. Resonant behavior and frequency preferences of thalamic neurons. *J. Neurophysiol.* 71: 575–582, 1994.

PUIL, E., MIURA, R. M., AND SPIGELMAN, I. Consequences of 4-aminopyridine applications to trigeminal root ganglion neurons. *J. Neurophysiol.* 62: 810–820, 1989.

SOLTESZ, I. AND CRUNELLI, V. A role for low-frequency, rhythmic synaptic potentials in the synchronization of cat thalamocortical cells. *J. Physiol. Lond.* 457: 257–276, 1992.

SOLTESZ, I., LIGHTOWLER, S., LERESCHE, N., JASSIK-GERSCHENFELD, D., POLLARD, C. E., AND CRUNELLI, V. Two inward currents and the transformation of low-frequency oscillations of rat and cat thalamocortical cells. *J. Physiol. Lond.* 441: 175–197, 1991.

SOONG, T. W., STEA, A., HODSON, C., DUBEL, S., VINCENT, S. R., AND SNUTCH, T. P. Structure and functional expression of a member of the low voltage-activated calcium channel family. *Science Wash. DC* 260: 1133–1136, 1993.

STERIADE, M., CURRÓ DOSSI, R. C., AND NUÑEZ, A. Network modulation of a slow intrinsic oscillation of cat thalamocortical neurons implicated in sleep delta waves: cortically induced sychronization and brainstem cholinergic suppression. *J. Neurosci.* 11: 3200–3217, 1991.

STERIADE, M., JONES, E. G., AND LLINÁS, R. R. *Thalamic Oscillations and Signalling.* New York: Wiley, 1990.

STRÖHMANN, B., SCHWARZ, D. W. F., AND PUIL E. Subthreshold frequency selectivity in avian auditory thalamus. *J. Neurophysiol.* In press.

TAKAHASHI, K. AND AKAIKE, N. Calcium antagonist effects on low-threshold (T-type) calcium current in rat isolated hippocampal CA1 pyramidal neurons. *J. Pharmacol. Exp. Theor.* 256: 169–175, 1991.

TRAUB, R. D., WONG, R. K., MILES, R., AND MICHELSON, H. B. A model of a CA3 hippocampal pyramidal neuron incorporating voltage-clamp data on intrinsic conductances. *J. Neurophysiol.* 66: 635–650, 1991.

WANG, X. J., RINZEL, J., AND ROGAWSKI, M. A. A model of the T-type calcium current and the low-threshold spike in thalamic neurons. *J. Neurophysiol.* 66: 839–850, 1991.

YAMADA, W. M., KOCH, C., AND ADAMS, P. Multiple channels and calcium dynamics. In: *Methods in Neuronal Modeling: From Synapses to Networks,* edited by C. Koch and I. Segev. Cambridge, MA: MIT Press, 1989, p. 97–133.